

Impact of Applying a Skin Compression With the Ultrasound Probe on Carotid Artery Strain Elastography

Boris Chayer, MSc, Marie-Hélène Roy Cardinal, PhD, Vicky Biron, BSc, Noémie Cloutier, BSc, Clara Petit, BSc, Samuel Dubord, BSc, Louise Allard, PhD, Guy Cloutier, PhD 

Received March 18, 2021, from the Laboratory of Biorheology and Medical Ultrasonics, University of Montreal Hospital Research Center (CRCHUM), Montréal, Québec, Canada (B.C., M.-Hène.R.C., V.B., S.D., L.A., G.C.); Collège André-Grasset, Montréal, Québec, Canada (N.C., C.P.); Institute of Biomedical Engineering, University of Montreal, Montréal, Québec, Canada (G.C.); and Department of Radiology, Radio-Oncology and Nuclear Medicine, University of Montreal, Montréal, Québec, Canada (G.C.). Manuscript accepted for publication May 4, 2021.

Boris Chayer and Marie-Hélène Roy Cardinal equivalent co-authorship.

The authors declare no conflict of interest.

Address correspondence to Guy Cloutier, Eng., PhD, Laboratory of Biorheology and Medical Ultrasonics, Centre de Recherche du Centre Hospitalier de l'Université de Montréal (CRCHUM), 900 St-Denis, suite R1.1.464, Montréal, QC, Canada, H2X 0A9.

E-mail: guy.cloutier@umontreal.ca

Abbreviations

C|ShS|, cumulated axial shear strain magnitude; CAS, cumulated axial strain; CAT, cumulated axial translation; CCA, common carotid artery; CLT, cumulated lateral translation; ICA, internal carotid artery; IMT, intima media thickness; LMM, linear mixed models; LSME, Lagrangian speckle model estimator; Max|ShS|, maximum axial shear strain magnitude; MaxAS, maximum axial strain; NIVE, noninvasive vascular elastography; PDC, predetermined compression; SP, standard practice; STD, standard deviation; SWE, shear wave elastography

Objective—To study the impact of varying the external compression exerted by the ultrasound probe when performing a carotid strain elastography exam.

Methods—Nine healthy volunteers (mean age 43 years \pm 13 years; 6 men) underwent a vascular ultrasound elastography exam using a custom made sound feedback handle embedding the probe, and allowing the sonographer to adjust the applied compression. A clinical standard practice (SP) force was first recorded, and then predetermined compression (PDC) forces were applied, ranging from 0 to 5 N for the left common carotid artery (CCA) or 2–12 N for the left internal carotid artery (ICA). Six carotid elastography features, namely maximum and cumulated axial strains, maximum and cumulated shear strains, cumulated axial translation, and cumulated lateral translation were assessed with noninvasive vascular elastography (NIVE) on near and far walls of carotids. The carotid intima media thickness (IMT) and diameter were also measured.

Results—All elastography features on the near wall of both CCA and ICA decreased statistically significantly as the PDC force increased; this association was also observed for half of the features on the far wall. Three NIVE features at the lowest PDC force (out of 72 that were tested) were statistically significantly different than values at the SP force. Overall, NIVE showed some variance to probe compression with linear regression slopes revealing changes of 10.1%–45.6% in magnitude over the whole compression range on both walls. The maximum IMT for the ICA near wall, and carotid lumen diameters of both CCA and ICA were statistically significantly associated with PDC forces; these features underwent a decrease of 10.2%, 36.2%, and 17.6%, respectively, over the whole range of PDC force increase. Other IMT measurements were not statistically significantly associated with applied PDC forces.

Conclusion—These results suggest the need of technical guidelines for carotid strain elastography. Using the lowest probe compression while allowing a good B-mode image quality is recommended to improve the robustness of NIVE measurements.

Key Words—carotid artery; probe compression; strain imaging; ultrasonography; vascular elastography

Noninvasive vascular strain elastography is used for assessing carotid deformations induced by the pulse pressure; strain measures the change in shape of materials under a stress condition. For a similar pulse pressure, less deformation or strain will

doi:10.1002/jum.15750

occur in stiffer arteries. Increased carotid artery stiffness has been associated with the presence of carotid artery plaque, the degree of atherosclerosis, and the incidence of stroke,¹ but carotid artery stiffness is only weakly associated with the intima-media thickness (IMT).² Carotid strain thus provides additional information to more commonly used IMT measurements.

In vascular strain elastography, compression with the ultrasound probe is not needed to generate tissue motion. However, probe compression during an examination may constrain the carotid wall and thus affect strain imaging. The last European Federation of Societies for Ultrasound in Medicine and Biology update on clinical practices made no recommendation on probe compression during extracorporeal vascular strain elastography exams.³ In their initiative to standardize ultrasound elastography methods, there was no mention either on how to perform carotid strain elastography studies.⁴ On the other hand, the American Society of Echocardiography guidelines for IMT measurements recommend using minimal compression with the probe.⁵

A previous study revealed that a compression smaller than 30 mmHg did not influence strain measurements on the common carotid artery (CCA).⁶ It was also showed that this pressure induced minimal variations of the CCA geometry. Details were not given on the method used to measure this compression. An exhaustive *ex vivo* and *in vivo* study on carotid and femoral artery's behavior showed that the presence of surrounding tissues reduced the mean circumferential stress of the carotid vessel wall by 70%.⁷ This corresponded to a 20% smaller stretch ratio compared to an untethered carotid. A cuff was designed in Kim et al⁸ to control the surrounding tissue compression applied on the brachial artery. With a peripheral compression on the forearm equal to the diastolic pressure, they found that arterial wall strain and strain rate increased by a factor of 10.

As far as we know, the impact of varying the applied force induced by the ultrasound probe on carotid strain imaging has not yet been studied. The variation of six wall translation and wall strain parameters under different pressures applied to internal and common carotid arteries of healthy volunteers was investigated. In addition to evaluate the impact of varying the probe compression force, the force used during the standard practice examination was also measured for comparison.

Materials and Methods

Study Protocol

This study was approved by the ethics committee of University of Montreal Hospital. Nine subjects, 6 men and 3 women (aged between 27 and 59 years old) without a history of carotid plaques, cardiovascular, or cerebrovascular diseases signed an informed consent form approved by the ethical committee. Ultrasound acquisitions were made according to the Mannheim consensus.⁹ Subjects were lying in supine position with their head rotated approximately 45° to the opposite side that was imaged, and the probe was held at an angle providing images of vessel walls as most as possible perpendicular to the ultrasound beam. Longitudinal view sequences of the left common and internal carotid arteries were recorded by an experienced radiology technologist (40 years of experience). Participants were asked to stop moving, breathing, and swallowing during ultrasound acquisitions to prevent movement artifacts. The bulb at the beginning was visible on the left of CCA acquisitions. Between 90 and 116 images (approximately 3 heartbeats) of 40 mm depth and 38 mm width were acquired in radiofrequency mode (RF-mode) using a Terason instrument (t3000cv, Teratech Corporation, Burlington, MA, USA) at a frame rate of 30 images per second with a linear array probe (model 12 L5).

The external force applied on the neck of participants with the ultrasound probe was monitored using a custom-made force monitoring handle designed according to Guerrero et al.¹⁰ It contained a 3D force/torque sensor (mini40, ATI industrial automation, Apex, NC, USA) encapsulated in an aluminum casing (Figure 1). A 3D attitude heading reference system (3DM-GX2, Lord Microstrain, Williston, VT, USA) was attached to the top of the handle to measure the probe angle relative to the vertical axis. An in-house C- software was developed using the ATI DAQ F/T C-library to calibrate and monitor the applied force. Before each measurement, the load cell was tarred vertically using the manufacturer calibration file. The software then compensated the weight of the probe according to the inclination of the handle. The average error on force measurements associated with the angle compensation was -0.05 ± 0.16 N.

The force monitoring handle measured the applied force in real-time at a sampling frequency of

10 Hz. CCA and internal carotid artery (ICA) RF acquisitions were performed using standard practice (SP), and the mean pressure applied by the technician was recorded for each participant. The SP force corresponds to the amount of probe compression the sonographer would normally use during a clinical exam. Then, to guide the technologist in applying a predetermined compression (PDC) force according to the protocol, a feedback sound was emitted by the control computer. The sound intensity and frequency were proportional to the difference between targeted and current forces; the maximum sound intensity could also be adjusted on computer speakers. A gauge showing targeted and current forces was also displayed on the computer screen for proper adjustment of the applied pressure.

Six different PDC forces were chosen for the CCA and ICA. The maximum forces for each vessel were rounded to the compression force corresponding to discomfort, as reported by a single volunteer during a pretest. Since different probe positioning is used for the CCA and ICA, different discomfort thresholds were measured for each of them. More pressure is usually required for the ICA to get a good imaging plane. Predetermined compression forces for the CCA were 0 N, 1 N, 2 N, 3 N, 4 N, and 5 N, whereas PDC forces

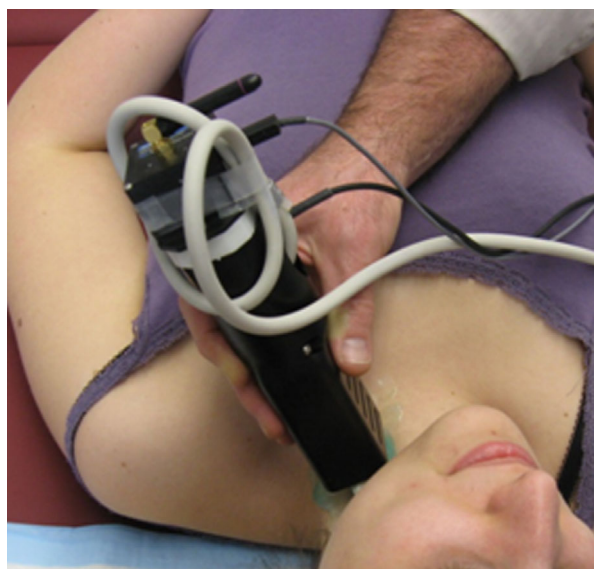
for the ICA were 2 N, 4 N, 6 N, 8 N, 10 N, and 12 N. Compression forces of 5 N and 12 N with the 6 cm² probe (approximated by considering the flat and curved portions of the linear array probe) correspond, respectively, to ≈ 62 mmHg and ≈ 150 mmHg. Participants could stop experiments if an applied force was too uncomfortable; in that case, forces higher or equal to their individual discomfort threshold were not further tested. To take into account within subject variability, three RF data acquisitions were recorded at the SP probe compression. Three replicates of each PDC force were also applied and acquired in random order. The CCA was always imaged before the ICA. Volunteers were asked to stand up 30 seconds between CCA and ICA exams to reduce blood pressure changes during examinations. Acquisitions started as soon as the participant lay down. The arterial blood pressure was measured with a brachial cuff before CCA series, before ICA series, and at the end of the experimentation. The mean pulse pressure (mean systolic pressure minus mean diastolic pressure) was computed for every participant. Normalization of strain indices based on measured blood pressure was not considered in this study.^{11,12}

Image Segmentation and Elastogram Computation

Radiofrequency ultrasound images were imported and analyzed with a commercial imaging platform (ORS Visual, Object Research Systems, Montréal, QC, Canada) using custom segmentation and elastography plugins. Figure 2 shows CCA reconstructed B-mode images and wall segmentations at 2 different PDC forces.

To initialize the automated segmentation of carotid walls, contours of both near and far walls were manually traced by an experienced technician on one image of each sequence. For CCA walls, measurements were made at least 5 mm before the bulb on a segment of at least 10 mm length. For ICA walls, measurements were made above flow divider and, if not feasible considering geometry and image quality, as far possible as above bulb widening. A segmentation method, combining approaches of Destrempes et al,^{13,14} was then used to detect contours on all remaining frames. Elastograms within segmented walls were computed between all pairs of consecutive images using the Lagrangian speckle model estimator (LSME).¹⁵ The affine-based LSME algorithm computes the tissue translation, strain, and shear strain

Figure 1. Custom-made force monitoring system designed to measure the force applied by the ultrasound probe on the participant's neck.



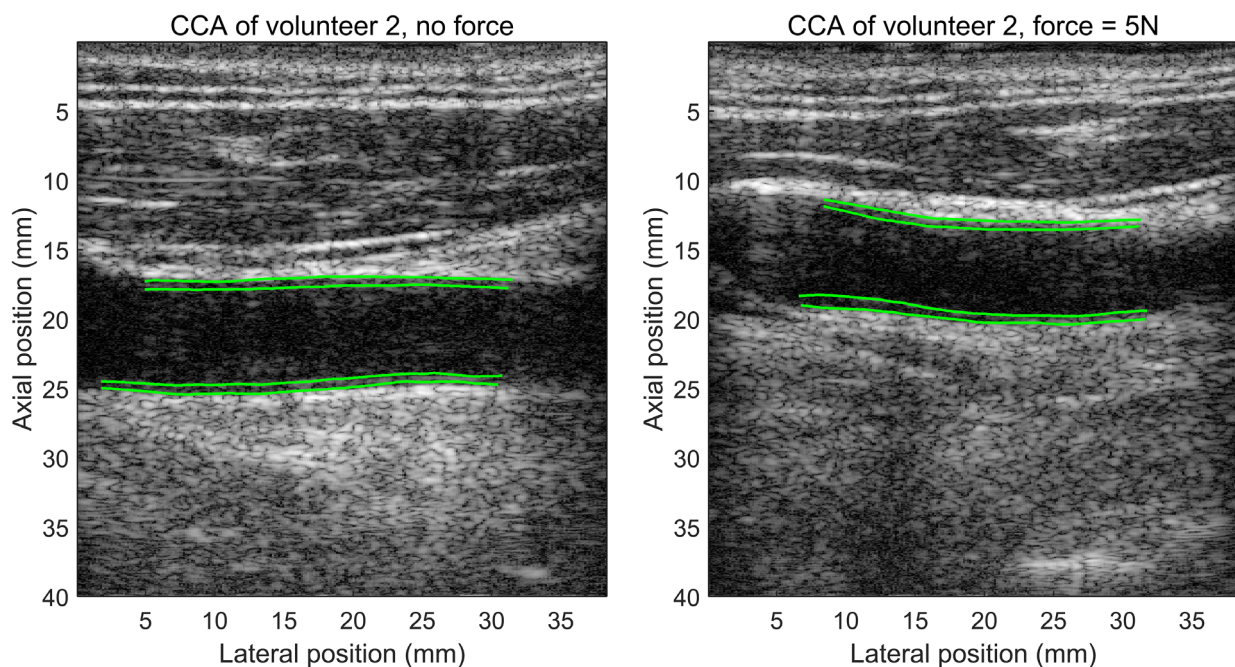
within measurement windows with an optical flow algorithm. Two-dimensional maps of all deformation components were produced by using a sliding measurement window over the segmented region. The translation refers to the rigid motion of the vessel wall. The strain corresponds to the compression and dilation of the vessel wall due to the varying blood pressure into the carotid artery. The shear deformation can be viewed as an angular change of shape of the structure produced by the blood pressure. Measurement windows of 2 mm axially and 3 mm laterally, and sliding overlaps of 95% axially and 80% laterally were used in this study.

Elastography components were computed axially, along the ultrasound beam, and laterally, along the length (long axis) of the probe. Elastography images were spatially averaged over the segmented wall region on each frame to produce instantaneous features that were then plotted as temporal curves. Reported maxima correspond to the maximum of instantaneous curves for each cardiac cycle that were averaged over available heartbeats.¹⁶ Cumulated curves were computed by summing instantaneous elastography features over each cardiac cycle. Cumulated features correspond to the

averaged range of those curves over all available cardiac cycles (a reset to zero was imposed at the end of each cycle).

Six strain, shear strain, and translation features are reported.^{17–19} They quantify different components of the vessel wall motion. The first two features are the maximum axial strain (MaxAS) and cumulated axial strain (CAS); they correspond respectively to the peak and global compression or dilatation of the vessel wall during a cardiac cycle. The next two features are the maximum axial shear strain magnitude (Max|ShS|) and cumulated axial shear strain magnitude (C|ShS|); they correspond to the peak and global angular change of shape inside the vessel wall during a cardiac cycle. The last two features are the cumulated axial translation (CAT) and cumulated lateral translation (CLT); they correspond to the total rigid displacement of the vessel wall during the cardiac cycle. All features were averaged over three cardiac cycles. Morphometric features computed from segmented carotid wall contours were also included in the analysis. The intima-media thickness (IMT) was evaluated on each frame as the averaged thickness of the segmented wall. Minimum and maximum

Figure 2. B-mode images of the common carotid artery (CCA) of a 52-year-old male volunteer with near and far walls segmentation in green. **A**, No compression (0 N) was applied by the radiology technologist, **B**, a predefined compression of 5 N was selected.



IMT over each cardiac cycle were then selected, and averaged over all cardiac cycles. Finally, the carotid lumen diameter was estimated as the distance between segmented near and far wall contours, and averaged over all frames.

Statistical Analysis

Elastography and morphometric features were analyzed separately for the CCA and ICA, and for near and far walls (except for carotid diameters). The results are described as mean \pm one standard deviation (STD). Outliers were removed by winsorizing each feature²⁰ (5th percentile and 95th percentile were used). Linear mixed models (LMM) were considered to evaluate the relation between elastography and morphometric features, and PDC forces. Independent variables accounting for cardiovascular confounding factors (continuous variables of age and pulse pressure; categorical variable of sex) were considered as fixed effects in the LMMs. The subjects repeated measurement was considered as an independent random effect; a random intercept for each subject was thus included in the LMM. To allow a comparison of slope estimates from different feature models, all variables were scaled between [0, 1]. The difference between elastography and morphometric measurements at the SP force versus each PDC force was evaluated with ANOVA analyses. When a statistically significant effect of the force factor in the ANOVA analysis occurred, the Dunnett multiple comparison test between the SP force (control

group) and each PDC force was applied. For the ANOVA analysis, the three repeated measures at each force for a given subject were averaged. The level of statistical significance was set at a *P*-value <0.05 . Statistical analysis was performed using *R* software (version 3.2.5; *R* Foundation for Statistical Computing, <https://www.r-project.org>).

Results

No participant indicated that PDC forces were uncomfortable. A total of 42 RF sequences were acquired for each subject on left common and internal carotids. One sequence showing movement artifacts on post-processing due to unexpected swallowing, even if participants were instructed to avoid it, was removed from the study. Population characteristics can be found in Table 1; a subject was considered hypertensive because of hypertension medication. Blood pressure and heart rate measurements that were made before, during, and after experimentations are found in Table 2. There was a statistically significant decrease of the systolic blood pressure during experimentations.

Figures 3 and 4 show the mean \pm SD of elastography features as a function of the PDC force applied by the probe on both near and far walls. Morphometric features on minimum IMT, maximum IMT, and lumen diameter are shown in Figure 5. The measured mean force corresponding to the standard practice (SP) for every participant was 2.60 ± 0.97 N (values between 1.0 N and 4.3 N) and 6.40 ± 1.58 N (values between 3.1 N and 10.0 N) for the CCA and ICA, respectively. Elastography and morphometric parameters for SP force series are shown by a single point \pm *x*-axis and *y*-axis SDs, with the color matched to the CCA (red) or ICA (green) series. LMMs confirmed statistically significant negative associations

Table 1. Population Characteristics

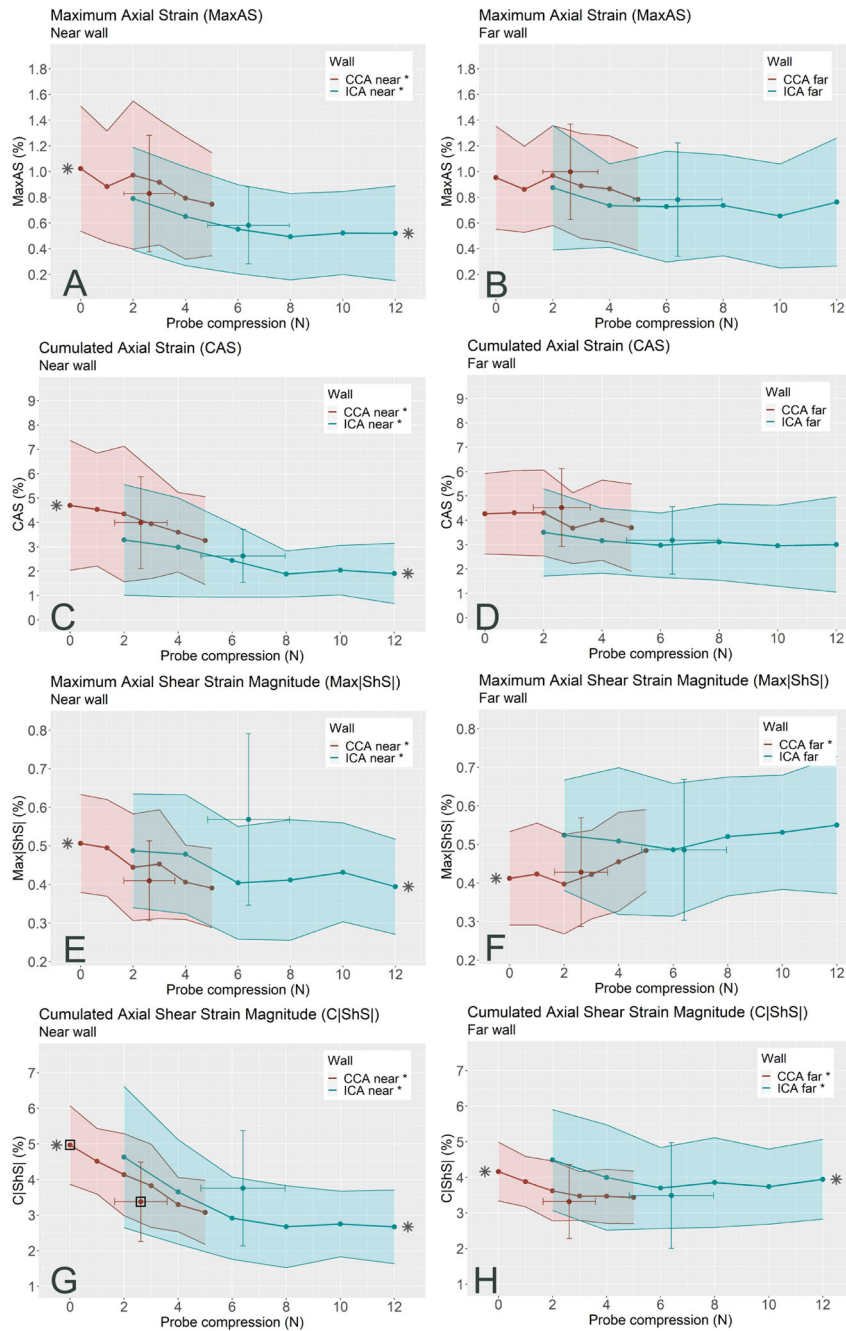
Number of participants	9
Age	43 \pm 13 years
Sex (male)	6 (67%)
Hypertension	1 (11%)

Table 2. Blood Pressure Measurements During Experimentations

	Before CCA Experimentation	Before ICA Experimentation	End of Experimentation	<i>P</i> Value
SBP	124 \pm 11	121 \pm 11	113 \pm 10	.049
DBP	74 \pm 10	74 \pm 10	67 \pm 6	.11
Pulse pressure (SBP-DBP)	50 \pm 11	47 \pm 10	46 \pm 10	.43
Heart beat	75 \pm 12	73 \pm 11	72 \pm 11	.67

P value from one-way ANOVA analysis in bold represents statistically significant results. SBP, systolic blood pressure; DBP, diastolic blood pressure.

Figure 3. Elastography strain features of the common and internal carotid arteries (CCA and ICA, respectively) for near (left column) and far (right column) walls plotted versus probe predetermined compression (PDC) forces. Each curve shows the mean value of the feature, whereas the shaded area represents its standard deviation. Curves that had significant mixed-model linear regressions are shown by * on their side (left side for CCA and right side for ICA); regression lines are not shown. Square (CCA) or pentagon (ICA) markers indicate significant differences between standard practice (SP) values and marked PDC force values. Elastography values at the SP force are shown by a single point \pm x-axis and y-axis standard deviations with the color corresponding to CCA (red) or ICA (green) series. SP error bars were computed over all acquisitions. **A** and **B**, maximal axial strain (MaxAS); **C** and **D**, cumulated axial strain (CAS); **E** and **F**, maximum shear strain magnitude (Max|ShS|); and **G** and **H**, cumulated shear magnitude (C|ShS|); all measures are in percent.



with PDC forces for each elastography feature on the near wall of both CCA and ICA, indicating that vessel wall strains (MaxAS, CAS, Max|ShS|, and C|ShS|) and translations (CAT and CLT) decreased as the probe compression increased. There were also statistically significant associations with PDC forces for the far CCA wall in the case of Max|ShS|, C|ShS|, CAT, and CLT; and for the far ICA wall for C|ShS| and CLT; these latter two features also decrease with

increase in probe compression. For morphometric features, the maximum IMT for the ICA near wall, and both carotid lumen diameters were statistically significantly associated with PDC forces; again these features decreased as the PDC force was increased. Features are expressed in % (MaxAS, CAS, Max|ShS|, C|ShS|) or mm (CAT, CLT, minimum IMT, maximum IMT, lumen diameter). Statistically significant associations presented in Table 3 (LMM results) are

Figure 4. Elastography translation features of the common and internal carotid arteries (CCA and ICA, respectively) for near (left column) and far (right column) walls plotted versus probe predetermined compression (PDC) forces. Each curve shows the mean value of the feature, whereas the shaded area represents its standard deviation. Curves that had significant mixed-model linear regressions are shown by * on their side (left side for CCA and right side for ICA); regression lines are not shown. Square (CCA) or pentagon (ICA) markers indicate significant differences between standard practice (SP) values and marked PDC force values. Elastography values at the SP force are shown by a single point ± x-axis and y-axis standard deviations with the color corresponding to the CCA (red) or ICA (green) series. SP error bars were computed over all acquisitions. **A** and **B**, cumulated axial translation (CAT); and **C** and **D**, cumulated lateral translation (CLT); all measures are in mm.

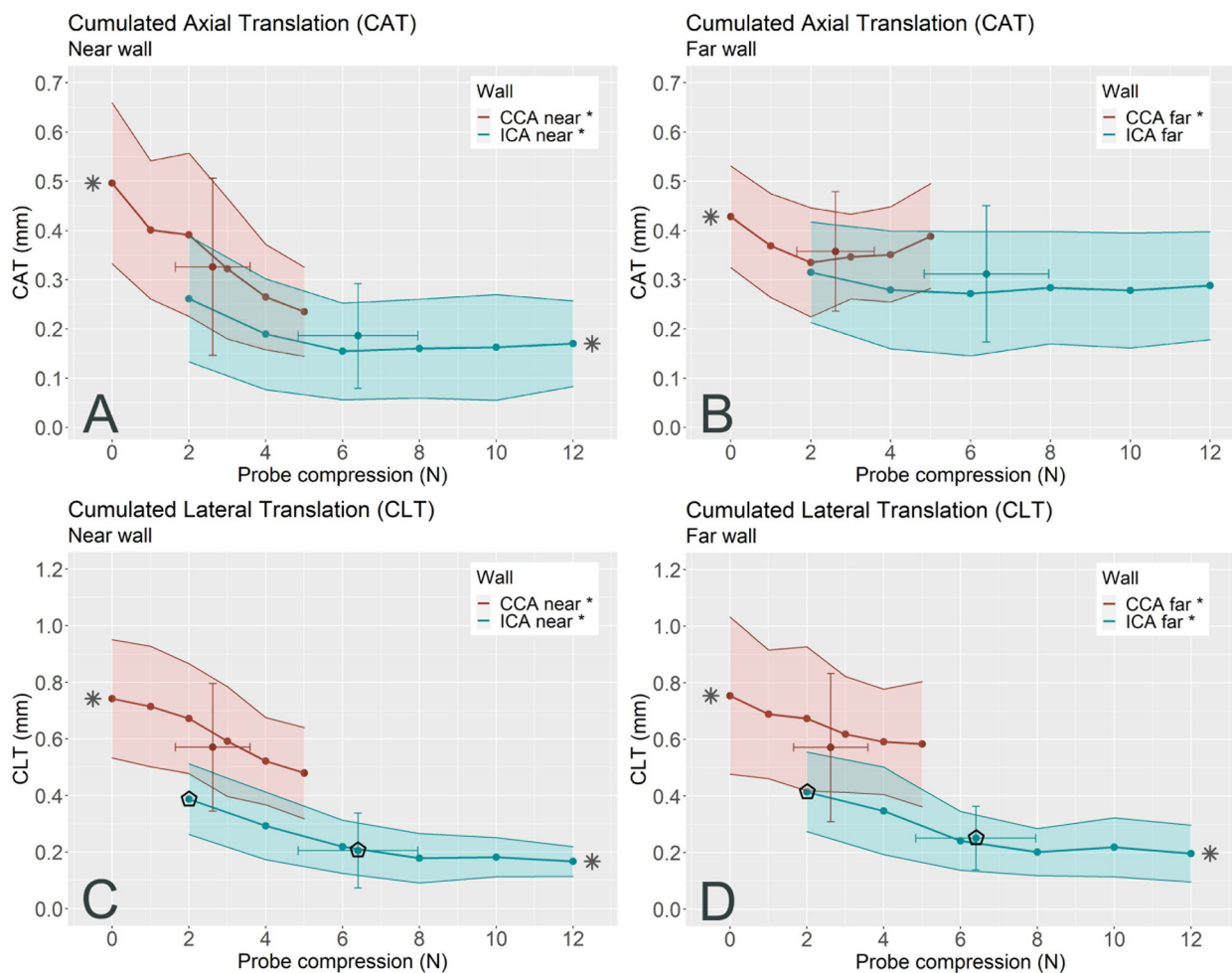
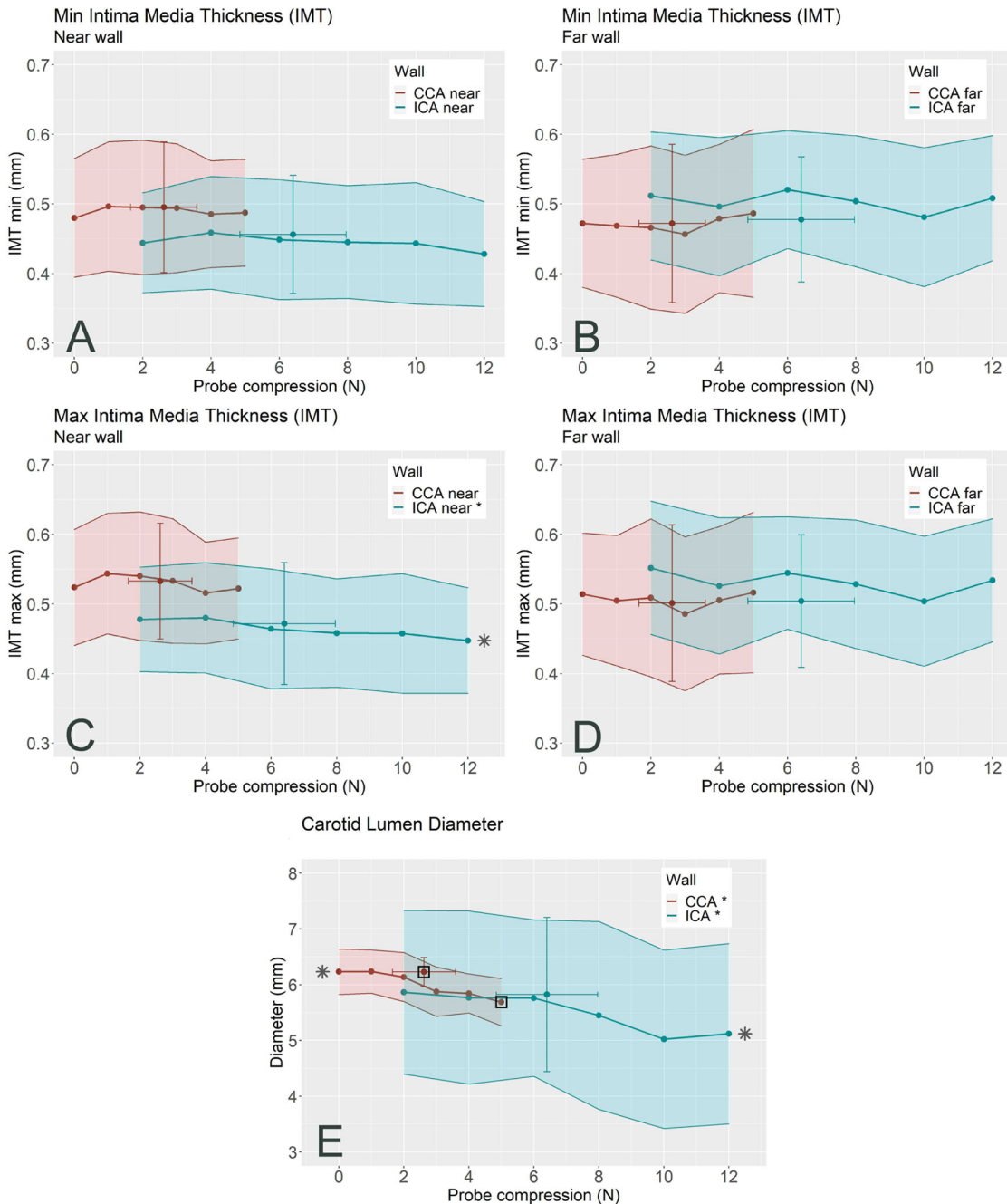


Figure 5. Morphometric features of the common and internal carotid arteries (CCA and ICA, respectively). Intima media thickness (IMT) features are presented for near (left column) and far (right column) walls plotted versus probe predetermined compression (PDC) forces. Diameters for the CCA and ICA are plotted versus probe PDC forces. Each curve shows the mean value of the feature, whereas the shaded area represents its standard deviation. Curves that had significant mixed-model linear regressions are shown by * on their side (left side for CCA and right side for ICA); regression lines are not shown. Square (CCA) or pentagon (ICA) markers indicate significant differences between standard practice (SP) values and marked PDC force values. Morphometric values at the SP force are shown by a single point \pm x-axis and y-axis standard deviations with the color corresponding to the CCA (red) or ICA (green) series. SP error bars were computed over all acquisitions. **A** and **B**, minimum intima media thickness (min IMT); **C** and **D**, maximum intima media thickness (max IMT); and **E**, carotid lumen diameter; all measures are in mm.



shown by * on the side of the corresponding curve in Figures 3–5.

Linear mixed-model slope estimates of the PDC force fixed effect on features for near and far CCA and ICA walls are given in Table 3. For statistically significant regression results, *P*-values and slope estimates (β) are presented in bold. The slope can be interpreted as the rate of change over the whole range of PDC forces since all variables were scaled between [0, 1]. According to these slope estimates with statistically significant results, decreases in elastography values between 10.1% and 45.6% were observed as the PDC force increased from its lowest to highest values. Max|ShS|, for the far CCA wall, is the only feature showing a statistically significant positive slope corresponding to a 15.5% increase over the whole PDC force range. In the LMMs model, each participant had a specific intercept (random factor) that accounted between 0% and 45% of the model variability for strain features, and between 15% and 37% for morphometric features.

One-way ANOVA with Dunnett multiple comparison tests were used to assess differences between

elastography and morphometric features at the SP compression and each PDC force. Details of the ANOVA analysis are given in Table 4. In multiple comparison

Table 4. *P* Values of the ANOVA Between Common and Internal Carotid Artery Elastography Features at the Standard Practice (SP) and Predetermined Compression (PDC) Forces

Feature	Carotid Wall			
	Near CCA	Far CCA	Near ICA	Far ICA
MaxAS	0.815	0.748	0.225	0.905
CAS	0.611	0.644	0.082	0.973
Max ShS	0.136	0.755	0.052	0.937
C ShS	2.54e–4	0.151	2.29e–3	0.610
CAT	3.19e–3	0.361	0.192	0.975
CLT	7.37e–3	0.461	6.42e–7	8.92e–6
Min IMT	0.999	0.999	0.978	0.793
Max IMT	0.997	0.998	0.937	0.690
Diameter	1.41e–3		0.661	

Values are shown for near and far walls except for diameter. *P* values in bold represent statistically significant results.

CCA, common carotid artery; ICA, internal carotid artery; MaxAS, maximum axial strain; CAS, cumulated axial strain; Max|ShS|, maximum axial shear strain magnitude; C|ShS|, cumulated axial shear strain magnitude; CAT, cumulated axial translation; CLT, cumulated lateral translation; IMT, intima media thickness.

Table 3. *P* Values of Fixed Factor Effect of Predetermined Compression (PDC) Forces on Elastography Features of the Common and Internal Carotid Arteries in the Linear Mixed-Model

Feature	Statistics	Carotid Wall			
		Near CCA	Far CCA	Near ICA	Far ICA
MaxAS	<i>P</i> -value	3.74e–03	0.099	6.66e–04	0.187
	β	–0.156		–0.199	
CAS	<i>P</i> -value	4.06e–04	0.080	8.34e–06	0.189
	β	–0.184		–0.222	
Max ShS	<i>P</i> -value	1.46e–07	2.06e–03	5.28e–03	0.426
	β	–0.246	0.155	–0.170	
C ShS	<i>P</i> -value	<2e–16	2.49e–07	8.91e–11	0.024
	β	–0.456	–0.278	–0.319	–0.118
CAT	<i>P</i> -value	<2e–16	4.98e–3	2.38e–04	0.255
	β	–0.442	–0.101	–0.190	
CLT	<i>P</i> -value	2.98e–13	9.92e–06	<2e–16	3.15e–14
	β	–0.384	–0.182	–0.474	–0.437
min IMT	<i>P</i> -value	0.971	0.262	0.171	0.448
	β				
max IMT	<i>P</i> -value	0.277	0.909	0.018	0.101
	β			–0.102	
Diameter	<i>P</i> -value	9.98e–15		1.84e–03	
	β	–0.362		–0.176	

Values are shown for near and far walls except for diameters. For statistically significant results, *P* values and slope estimates (β) are reported in bold.

CCA, common carotid artery; ICA, internal carotid artery; MaxAS, maximum axial strain; CAS, cumulated axial strain; Max|ShS|, maximum axial shear strain magnitude; C|ShS|, cumulated axial shear strain magnitude; CAT, cumulated axial translation; CLT, cumulated lateral translation; IMT, intima media thickness.

tests, statistically significant differences versus SP values occurred at the lowest PDC force of 0 N for C|ShS| in the near wall of the CCA ($P = .0037$); and of 2 N for CLT in the near and far walls of the ICA ($P = 6.60e-5$ and $P = 2.50e-3$, respectively). A statistically significant difference was also observed at the highest PDC force of 5 N for the CCA diameter ($P = 5.90e-3$). Square (CCA) or pentagon (ICA) markers depicted in Figures 3–5 indicate these statistically significant differences between SP values and marked PDC force values.

Discussion

A custom-made force monitoring handle embedding the ultrasound probe was used to evaluate the relation between the compression applied on the skin during ultrasound examination, and carotid elastography and morphometric features. As shown in Table 2, blood pressure measurements decreased over time, but only the systolic blood pressure statistically significantly changed during the experiments. As SP measurements were made before PDC ones, the blood pressure drop could emphasize differences when comparing them. Moreover, comparisons between CCA and ICA measurements could also be affected by this blood pressure effect because they were made one after the other. Still, to prevent the confounding effect of blood pressure drop over time, PDC measurements were made in random order, as mentioned in the Methods section, so the reported trends were not affected by this.

The effect of the applied force by the probe was found to affect all elastography features (Table 3). Carotid diameters were also affected, but there was almost no impact on IMT measurements, except for the near wall maximum IMT ICA values. When compared with the results at SP compressions (Table 4), only a few features at extreme applied forces differed among multiple comparisons.

As noticed in Tables 3 and 4, the probe compression mainly affected features of the near wall. As the far wall is farther from the probe, elastography and IMT measures were less influenced by the probe compression, likely due to the blood flow that could act as a barrier between the applied force and the far wall. The far wall was nonetheless affected. As expected, CCA and ICA diameters decreased as the

PDC increased. A reduced artery motion in the imaging plane was also observed in Table 3 (slope estimates (β) ranged between -0.474 and -0.101 for translation features CAT and CLT on both walls). Axial strain features (MaxAS and CAS) decreased only for the near wall. It was also observed that only the maximum IMT for the near ICA wall decreased with increasing compression. As most IMT measurements did not statistically significantly change over applied PDC forces, a higher sample size might be needed to see an effect on low magnitude IMT changes. Since the artery was constrained only in one direction radially but actually beats radially in 3D, the reduced motion in the longitudinal view plane could have been compensated by an increased motion in other radial directions (as would be seen in a transverse view). Unfortunately, the radial motion could not be investigated with this experimental setup. Finally, strain decay in the neck tissue, where the effect of the probe compression decreases with depth,²¹ in part likely explains the lesser impact of the probe compression on the far wall.

Table 3 shows that mainly negative statistically significant associations were found with the probe applied force, indicating that strain features decreased as the probe compression increased. One exception was Max|ShS| for the far CCA wall, where an increase was observed. Still, C|ShS| for the same wall decreased with a higher magnitude than the Max|ShS| increased. The Max|ShS| feature of other walls was either negatively or not statistically significantly associated with PDC forces. As shear strain is related to an angular change of shape, the nature of this change might not have been completely captured with our experiments. Sample size, variability of instantaneous measurements, and the two-dimensional view of the walls could explain this contradicting behavior.

As noticed in Figure 5, the variability of lumen diameter measurements was higher for the ICA than the CCA. The tortuosity and deep penetration angle of the ICA could partly explain this variability. Since it was not always possible to obtain a straight segment past the bulb widening, the variability could also result from ICA measurements that were made more or less close to the carotid bulb, where the diameter is much higher than the CCA and ICA.²²

To compensate for the blood pressure within the brachial artery in the context of wall strain

measurements, Kim et al applied an external compression with a pressure cuff inducing a force equivalent to the diastolic blood pressure (typically 80 mmHg).⁸ Under this condition, they did not observe a reduction but a strong enhancement of the radial intramural strain, contrary to our results obtained using a local probe compression. The external probe compression used in the current study (6 N with the probe corresponds to ≈ 75 mmHg) was in the same range as the cuff surrounding the arm in Kim et al,⁸ but the probe compression constrained the motion in one direction only (axially, along the applied force axis) contrary to the arm cuff induced constraint that was in all radial directions. Due to different imposed boundary conditions, trends similar to Kim et al⁸ were thus not expected in our study. It is nevertheless of interest to notice the opposite effect on strain of a force imposed by a cuff instead of a probe.

Standard Practice Measurements

The location, tortuosity, and 3D projection with depth of the internal carotid artery required an extra compression during the clinical examination to get a proper longitudinal imaging view. When imaging the CCA, the probe is positioned in a smoother section of the neck compared to imaging the ICA, where the probe is closer to the jaw. Indeed, the average SP force used during ICA scans (6.4 N) was higher than that used on the CCA (2.6 N). The discomfort thresholds established during a pretest were also higher for the ICA than CCA. The SP force measured in this study represents the practice of a single radiology technologist and cannot be generalized, but since PDC forces varied between no force and a uncomfortable force, it is believed that the force used in clinics by different radiology technologists would be in that range. It is likely easier for the radiology technologist to keep the probe stable and avoid movement during an acquisition if a small pressure is applied on the skin.

In Table 4, we observed statistically significant influences of the probe compression on elastography features, mostly when the applied force was either in the lowest or highest value of selected PDC forces when compared with SP forces. These statistically significant differences were also observed more frequently on the near wall. Since normalizing the applied pressure during clinical scans might be

difficult without using a force feedback sensor system, as developed here, keeping a minimum probe compression while obtaining an acceptable image quality is recommended to avoid confounding effects on elastography features. In cases where a higher probe pressure is required to scan a subject, especially for the ICA, a qualitative categorical evaluation (e.g., high probe pressure necessary: yes or no) might be added to the exam to consider it as a confounder in statistical analysis of elastography features.

As mentioned previously, no clear guideline currently exists on how the probe pressure should be applied during vascular strain elastography exams. It should be noticed, however, that studies using shear wave elastography (SWE) on superficial tissues (skin, fascia, tendon, and muscle) recommended using the lowest possible pre-compression to avoid incorrect measurements.^{23–26} Interestingly, higher stiffness was measured in both malignant and benign breast when compression increased²⁷; applying a mild probe compression nevertheless increased the diagnostic accuracy. These different practices show the relevance of specific technical guidelines regarding probe compression adapted to different clinical elastography examinations.

Limitations

The participant number, 9, is a limitation of this study; this low number could explain the contradicting trend observed for the Max|ShS| feature. In addition, since only healthy carotid arteries from participants with normal body mass indices were studied, future works should be done on atherosclerotic arteries using the sound feedback probe handle to validate reported observations on patients with carotid plaques. A cross-sectional view of the carotid during compression with a longitudinal oriented device would be necessary to capture the motion in all directions under our probe compression conditions. A final limitation of this study was that the increased weight and size of the ultrasound probe, caused by the addition of the custom-made force monitoring, might have changed the operating conditions; however, the modified probe size was close to the previous generation of ultrasound probes, and did not prevent the technologist from producing ultrasound acquisitions with quality comparable to a clinical examination.

Conclusion

We studied the effect of different external ultrasound probe compressions on common and internal carotid artery strain elastography features. Linear mixed models showed that increasing the probe compression decreased the vessel wall movement (i.e., axial and lateral translations), and the wall deformation characterized by various strain and shear strain features. The probe compression mainly impacted CCA and ICA near walls. Compared with the compression applied by an expert technician, elastography features differed when low or high compression levels were used. Almost no effect of the probe compression was observed on IMT measures. Since monitoring the probe pressure might be difficult in the clinical context, we recommend using a minimum pressure during carotid strain elastography exams.

Acknowledgements

This study was initiated through the financial support of the Collaborative Health Research Program of the Natural Sciences and Engineering Research Council of Canada (#462240-14) and Canadian Institutes of Health Research (#CPG-134748). It is now supported by the Canadian Institutes of Health Research (#399544). The authors acknowledge the contribution of Michel Gouin for performing ultrasound data acquisitions, and Zhao Qin for carotid artery wall segmentation.

References

- Boesen ME, Singh D, Menon BK, Frayne R. A systematic literature review of the effect of carotid atherosclerosis on local vessel stiffness and elasticity. *Atherosclerosis* 2015; 243:211–222. <https://doi.org/10.1016/j.atherosclerosis.2015.09.008>.
- Riley WA, Evans GW, Sharrett AR, Burke GL, Barnes RW. Variation of common carotid artery elasticity with intimal-medial thickness: the ARIC study. *Atherosclerosis risk in communities. Ultrasound Med Biol* 1997; 23:157–164. [https://doi.org/10.1016/s0301-5629\(96\)00211-6](https://doi.org/10.1016/s0301-5629(96)00211-6).
- Săftoiu A, Gilja OH, Sidhu PS, et al. The EFSUMB guidelines and recommendations for the clinical practice of elastography in non-hepatic applications: update 2018. *Ultraschall Med* 2019; 40:425–453. <https://doi.org/10.1055/a-0838-9937>.
- Dietrich CF, Barr RG, Farrokh A, et al. Strain Elastography—how to do it? *Ultrasound Int Open* 2017; 3:E137–E149.
- Stein JH, Korcarz CE, Hurst RT, et al. Use of carotid ultrasound to identify subclinical vascular disease and evaluate cardiovascular disease risk: a consensus statement from the American Society of Echocardiography carotid intima-media thickness task force endorsed by the Society for Vascular Medicine. *J Am Soc Echocardiogr* 2008; 21:93–111. <https://doi.org/10.1016/j.echo.2007.11.011>.
- Kanai H, Hasegawa H, Ichiki M, Tezuka F, Koïwa Y. Elasticity imaging of atheroma with transcutaneous ultrasound: preliminary study. *Circulation* 2003; 107:3018–3021.
- Liu Y, Dang C, Garcia M, Gregersen H, Kassab GS. Surrounding tissues affect the passive mechanics of the vessel wall: theory and experiment. *Am J Physiol Heart Circ Physiol* 2007; 293:H3290–H3300. <https://doi.org/10.1152/ajpheart.006666.2007>.
- Kim K, Weitzel WF, Rubin JM, Xie H, Chen X, O'Donnell M. Vascular intramural strain imaging using arterial pressure equalization. *Ultrasound Med Biol* 2004; 30:761–771.
- Touboul PJ, Hennerici MG, Meairs S, et al. Mannheim carotid intima-media thickness and plaque consensus (2004-2006-2011). An update on behalf of the advisory board of the 3rd, 4th and 5th watching the risk symposia, at the 13th, 15th and 20th European stroke conferences, Mannheim, Germany, 2004, Brussels, Belgium, 2006, and Hamburg, Germany, 2011. *Cerebrovasc Dis* 2012; 34: 290–296. <https://doi.org/10.1159/000343145>.
- Guerrero J, Salcudean SE, McEwen JA, Masri BA, Nicolaou S. System for deep venous thrombosis detection using objective compression measures. *IEEE Trans Biomed Eng* 2006; 53:845–854. <https://doi.org/10.1109/tbme.2005.863878>.
- Varghese T, Meshram NH, Mitchell CC, Wilbrand SM, Hermann BP, Dempsey RJ. Lagrangian carotid strain imaging indices normalized to blood pressure for vulnerable plaque. *J Clin Ultrasound* 2019; 47:477–485.
- Maurice RL, Soulez G, Giroux MF, Cloutier G. Non-invasive vascular elastography for carotid artery characterization on subjects without previous history of atherosclerosis. *Med Phys* 2008; 35: 3436–3443.
- Destrempe F, Meunier J, Giroux MF, Soulez G, Cloutier G. Segmentation in ultrasonic B-mode images of healthy carotid arteries using mixtures of Nakagami distributions and stochastic optimization. *IEEE Trans Med Imaging* 2009; 28:215–229. <https://doi.org/10.1109/tmi.2008.929098>.
- Destrempe F, Meunier J, Giroux M-F, Soulez G, Cloutier G. Segmentation of plaques in sequences of ultrasonic B-mode images of carotid arteries based on motion estimation and a Bayesian model. *IEEE Trans Biomed Eng* 2011; 58:2202–2211. <https://doi.org/10.1109/tbme.2011.2127476>.
- Mercure E, Cloutier G, Schmitt C, Maurice R. Performance evaluation of different implementations of the Lagrangian speckle model

- estimator for non-invasive vascular ultrasound elastography. *Med Phys* 2008; 35:3116–3126.
16. Mercure E, Destrempe F, Roy Cardinal MH, et al. A local angle compensation method based on kinematics constraints for non-invasive vascular axial strain computations on human carotid arteries. *Comput Med Imaging Graph* 2014; 38:123–136. <https://doi.org/10.1016/j.compmedimag.2013.08.005>.
 17. Cloutier G, Roy Cardinal M-H, Ju Y, Giroux M-F, Lanthier S, Soulez G. Carotid plaque vulnerability assessment using ultrasound elastography and echogenicity analysis. *AJR Am J Roentgenol* 2018; 211:847–855. <https://doi.org/10.2214/AJR.17.19211>.
 18. El Jalbout R, Cloutier G, Roy-Cardinal MH, et al. The value of non-invasive vascular elastography (NIVE) in detecting early vascular changes in overweight and obese children. *Eur Radiol* 2019; 29:3854–3861. <https://doi.org/10.1007/s00330-019-06051-9>.
 19. Roy Cardinal MH, Durand M, Chartrand-Lefebvre C, et al. Increased carotid artery wall stiffness and plaque prevalence in HIV infected patients measured with ultrasound elastography. *Eur Radiol* 2020; 30:3178–3187. <https://doi.org/10.1007/s00330-020-06660-9>.
 20. Wilcox RR. *Introduction to Robust Estimation and Hypothesis Testing*. 3rd Edition. Elsevier, New York: Academic Press; 2012.
 21. Souchon R, Soualmi L, Bertrand M, Chapelon JY, Kallel F, Ophir J. Ultrasonic elastography using sector scan imaging and a radial compression. *Ultrasonics* 2002; 40:867–871. [https://doi.org/10.1016/s0041-624x\(02\)00228-7](https://doi.org/10.1016/s0041-624x(02)00228-7).
 22. Kamenskiy AV, Pipinos II, Carson JS, MacTaggart JN, Baxter BT. Age and disease-related geometric and structural remodeling of the carotid artery. *J Vasc Surg* 2015; 62:1521–1528. <https://doi.org/10.1016/j.jvs.2014.10.041>.
 23. Kot BC, Zhang ZJ, Lee AW, Leung VY, Fu SN. Elastic modulus of muscle and tendon with shear wave ultrasound elastography: variations with different technical settings. *PLoS One* 2012; 7:e44348.
 24. Alfuraih AM, O'Connor P, Hensor E, Tan AL, Emery P, Wakefield RJ. The effect of unit, depth, and probe load on the reliability of muscle shear wave elastography: variables affecting reliability of SWE. *J Clin Ultrasound* 2018; 46:108–115.
 25. Rominger MB, Kálin P, Mastalerz M, et al. Influencing factors of 2D shear wave Elastography of the muscle - an ex vivo animal study. *Ultrasound Int Open* 2018; 4:E54–E60.
 26. Wang X, Hu Y, Zhu J, et al. Effect of acquisition depth and precompression from probe and couplant on shear wave elastography in soft tissue: an in vitro and in vivo study. *Quant Imaging Med Surg* 2020; 10:754–765.
 27. Hangard C, Gennisson JL, Reinhold C, Fournier LS. Diagnostic accuracy of four levels of manual compression applied in supersonic shear wave elastography of the breast. *Acad Radiol* 2020; 28(4):481–486. <https://doi.org/10.1016/j.acra.2020.03.012>.